Asian Journal of Chemistry; Vol. 35, No. 11 (2023), 2773-2781

ASIAN JOURNAL OF CHEMISTRY

https://doi.org/10.14233/ajchem.2023.30583

Ion Fluence-Dependent Structural and Electrical Characteristics of Electrochemically Synthesized PANI/ZnO Nanocomposites

AASIM HUSSAIN[1], SAMEEN AHMED KHAN[2], FARHA JABEEN[1], MOHD WARISH[1], INDRA SULANIA[3], ANJU DHILLON[4] and AZHER M. SIDDIQUI[1,*]

[1]Department of Physics, Jamia Millia Islamia, New Delhi-110025, India
[2]Department of Mathematics and Sciences, College of Arts and Applied Sciences, Dhofar University, Salalah, Sultanate of Oman
[3]Inter University Accelerator Centre, New Delhi-110067, India
[4]Department of Applied Sciences, Maharaja Surajmal Institute of Technology, New Delhi-110058, India

*Corresponding author: E-mail: amsiddiqui@jmi.ac.in

Received: 8 September 2023; *Accepted*: 10 October 2023; *Published online*: 31 October 2023; AJC-21435

The electrochemical synthesis and ion irradiation effects of polyaniline/zinc oxide (PANI/ZnO) nanocomposite films on stainless steel substrates were investigated in this study. The structural, morphological and electrical properties of the films were characterized by Raman spectroscopy, Fourier transform infrared spectroscopy (FTIR), scanning electron microscopy with energy dispersive spectroscopy (SEM-EDS) and current-voltage (I-V) measurements. The results show that the films have a nanofiber network structure with an average diameter of 50-60 nm. The vibrational modes and structural properties of the films are influenced by ion fluence. The electrical conductivity and mobility of the films increase significantly at low fluence (1.0×10^{11} ions/cm^2), reaching values of 1.14×10^{-2} S/cm and 3.56×10^{-5} cm^2/V-s, respectively. However, at high fluence, electrical properties degrade due to the damage caused by the ion irradiation. This study demonstrates the potential of PANI/ZnO nanocomposite films for applications in the optoelectronic devices and energy storage devices.

Keywords: Conducting polymers, Electrodeposition, PANI/ZnO, Nanocomposites, Irradiation.

INTRODUCTION

The idea of combining materials has been adopted in modern times and the main purpose is to improve the physical and chemical properties of individual materials to achieve specific goals that individual materials cannot accomplish. A variety of industrial applications have been explored by doping conjugated polymers with different metal oxides such as SnO_2, ZnO, TiO_2. Devices such as sensors, super capacitors, batteries, solar panels, electromagnetic shielding, actuators and electronic devices fall under this category [1,2].

A wide range of conductivity polymers are available, such as polypyrrole (PPy), polythiophene (PT), poly(3,4-ethylenedioxythiophene) (PEDOT), polyaniline (PANI), poly(*p*-phenylene vinylene) (PPV). Environmental stability, simplicity of synthesis, electronic conductivity and suitability for building composite materials with various substrates and binders have made polyaniline (PANI) an extremely popular material in recent years [3]. PANI is a conductive polymer that has a conjugated backbone of alternating single and double bonds between carbon atoms. PANI can switch between different oxidation states and colours depending on the doping level and the applied voltage. It has remarkable electrical properties, such as a wide range of conductivity (from 10^{-10} to 10^4 S/cm) upon doping, a high Seebeck coefficient (up to 100 μV/K) and a high thermoelectric power factor (up to 10^{-3} W/mK^2) [4]. PANI also has excellent redox reversibility, which means it can maintain its conductivity and structure after repeated oxidation and reduction cycles. PANI has decent chemical and environmental stability, which means it can resist degradation by acids, bases, oxidants, reductants and UV light. PANI has easy preparation process, which means it can be synthesized by chemical or electrochemical methods in various forms, such as powders, films, nanofibers, nanowires, nanotubes and nanoparticles [1,3].

Zinc oxide is a metal oxide that has many advantages over other metal oxides. It has high electron mobility, due to which

it can transfer electric charges faster and more efficiently than other metal oxides [5]. Zinc oxide has strong room-temperature luminescence, which means it can emit light when excited by an electric field or a laser. This makes it useful for transparent electrodes, light emitting diodes, transistors, sensors, displays and lasers [6].

PANI/ZnO nanocomposite are materials that combine PANI and ZnO nanoparticles in different ratios and configurations. These nanocomposites have synergetic effects on their electrical, optical, magnetic and catalytic properties, which are influenced by the interaction between PANI and ZnO nanoparticles. PANI/ZnO nanocomposite have higher conductivity than pure PANI or pure ZnO due to the charge transfer between PANI chains and ZnO nanoparticles. PANI/ZnO nanocomposite can have lower band gap than pure ZnO due to the formation of hybrid states between PANI orbitals and ZnO valence band. PANI/ZnO nanocomposite can have enhanced magnetization than pure PANI or pure ZnO due to the exchange coupling between PANI radicals and ZnO defects [7]. PANI/ZnO nanocomposite can have improved photocatalytic activity than pure ZnO due to the sensitization of PANI to visible light and the separation of photogenerated carriers by PANI/ZnO heterojunctions [8].

The PANI/ZnO nanocomposite films are synthesized by electrodeposition, which is a technique that uses an electric potential or current to deposit PANI and ZnO nanoparticles on a substrate, such as glassy carbon, stainless steel or indium tin oxide [9]. Electrodeposition is a simple, fast and low-cost technique that can control the morphology, thickness and composition of the nanocomposite film by adjusting the parameters such as voltage, current, time and concentration. Electrodeposition can also enhance the adhesion, stability and conductivity of the nanocomposite film on the substrate by forming a strong bond between the film and the substrate. Electrodeposition can also improve the properties and performance of the nanocomposite film for various applications, such as sensors, supercapacitors, photocatalysts and optoelectronics [10].

A novel method to modify the structure and properties of PANI/ZnO nanocomposite is swift heavy ion irradiation, which is a technique that uses high-energy ions to create cylindrical tracks of damage along their paths in the target material [11, 12]. Swift heavy ion irradiation is a powerful technique that can modify the structure and properties of polymer composites at the nanoscale level, while low energy ion beams can only affect the surface layer of the material. Swift heavy ion irradiation can create new functionalities and features in the nanocomposite film, such as luminescence, electrochromism and memory effects, while low energy ion beams can only induce defects and damage in the material. Swift heavy ion irradiation can enhance the electrical, optical, magnetic and catalytic properties of the nanocomposite film by inducing changes in the chemical composition, crystal structure, defect density and surface morphology of the material [13-15], while low energy ion beams can only reduce or degrade these properties. Swift heavy ion irradiation can control the extent and nature of the modification in the nanocomposite film by adjusting the parameters such as ion energy, fluence and species [16].

In this study, the effects of 100 MeV Ag^{10+} ions irradiation on PANI/ZnO nanocomposite fabricated electrochemically were investigated. According to stopping and range of ions in matter (SRIM) software, the irradiation energy was calculated so that the projected range of Ag^{10+} ions was considerably longer than the nanocomposite film thickness, resulting in uniform losses in electronic energy for the ions. Various techniques such as Raman spectroscopy, FTIR, SEM-EDS and electrical measurement dark I-V study were used to characterize the structural, morphological and electrical properties of the nanocomposite film before and after irradiation. The results of the pristine PANI/ZnO nanocomposites with PANI/ZnO nanocomposites irradiated at various fluences. The possible mechanisms and implications of the irradiation induced modification in the nanocomposite film for various applications. Pristine PANI/ZnO nanocomposite named S0 and irradiated PANI/ZnO nanocomposite films at ion fluences of 1×10^{10} and 1×10^{11} and 1×10^{12} ions/cm^2 named S1, S2 and S3, respectively.

The aim of this study is to explore the potential of swift heavy ion irradiation as a novel technique to tailor the properties and performance of PANI/ZnO nanocomposite for various applications. This study will provide new insights and perspectives on the design and fabrication of advanced polymer composites with enhanced functionalities and features.

EXPERIMENTAL

Aniline monomer (> 99% purity), zinc oxide nanoparticles, sulphuric acid, ethanol, *etc*. were procured from Sigma-Aldrich, USA. Throughout the experiment, double-distilled aniline monomer was used and deionized water was used to prepare all the solutions.

Electrodeposition of PANI/ZnO nanocomposite: PANI/ZnO films were fabricated by the chronopotentiometry technique on stainless steel (grade-304) substrate using the CHI660d electrochemical workstation, which consists of three electrodes. In this system, graphite as a counter electrode, stainless steel (SS) as a working electrode and standard calomel electrode as a reference electrode. The electrolyte solution (50 mL) composed of 0.2 M aniline and 0.45 M H_2SO_4 and 50 mg ZnO powder added to it [17]. During the preparation method, the constant current density (1 mA/cm^2) was applied to the working electrode for 300 s. One can prepare electrolyte solution for PANI films without adding ZnO powder in the solution while keeping the other parameters same as in PANI/ZnO polymerization.

Swift heavy-ion (SHI) irradiation of PANI/ZnO nanocomposite: A 15 UD pelletron accelerator at IUAC, New Delhi was used to irradiate electrochemically deposited thin films on stainless steel (SS) substrates of size 1 cm × 1 cm. An Ag^{10+} ion beam was irradiated in the materials science beamLine using three diffe-rent fluences of 1.0×10^{10}, 1.0×10^{11} and 1.0×10^{12} ions/cm^2 at 100 MeV. In order to increase fluence, the irradiation time was extended while the incident beam current remained at 0.3 pna (particle-nanoampere). In order to avoid excessive burning of conducting polymers, the fluence was limited to 1.0×10^{12} ions/cm^2. A calculation was made using SRIM software in which the projected range of Ag^{10+} ions would

be considerably longer than the nanocomposite film thickness, resulting in uniform loss of electronic energy.

Shimadzu's IRAffinity-1S were used to observe Fourier transform infrared (FTIR) patterns between 2500 and 650 cm^{-1}. Raman spectra were recorded with an Invia Renishaw spectrometer. A MIRA TESCAN operated at a 25kV accelerating voltage was used to capture scanning electron micrographs of pristine and irradiated PANI/ZnO nanocomposite. The I-V studies were performed at room temperature using Agilent Technologies, B1500A semiconductor device analyzer.

RESULTS AND DISCUSSION

FTIR studies: Fig. 1a-d displays the Fourier transform infrared (FTIR) spectrum of pristine and irradiated PANI/ZnO nanocomposite thin films. The existence of ZnO is confirmed by the absorption peaks at 576 and 505 cm^{-1}, which correspond to the stretching vibrations of Zn–O [18]. The band at 505 cm^{-1} exhibits a noticeable shift in the spectra for samples S2 and S3. Additionally, there were observable shifts towards lower wavenumbers in the IR absorption bands corresponding to angular deformations out of the plane of C-H bonds, which were detected at approximately 804 and 713 cm^{-1}. These shifts were particularly prominent in the films irradiated with doses exceeding 1×10^{10} ions/cm^2. The observed shifts can be ascribed to the existence of monosubstituted aromatic compounds inherent in the aniline monomer constituting the PANI structure.

Moreover, the confirmation of the characteristic ZnO peak at 885 cm^{-1} further validates the successful integration of ZnO NPs into the molecular structure of PANI [19]. The presence of the peak at 1139 cm^{-1} can be attributed to the C-H in-plane bending mode of benzoid rings and it is noteworthy that this peak exhibited a shift in its wavenumber for samples S2 and S3. This shift towards lower wavenumbers can be attributed to the formation of hydrogen bonds between the NH group of PANI and ZnO. The band detected at 1249 cm^{-1} is associated with the protonated C-N group [20,21]. Furthermore, the band observed at 1298 cm^{-1} can be attributed to the C-N stretching bond of the aromatic amines present in PANI [22]. Additionally, the distinctive peaks at 1572 and 1490 cm^{-1} have been assigned to the stretching modes of the C=C bonds in the benzenoid ring and the quinoid ring, respectively.

Raman spectroscopic studies: Fig. 2 displays the Raman spectra of PANI/ZnO nanocomposite thin films excited by a 532 nm laser. As depicted in Fig. 2b, in case of the pristine sample (S0), the observed bands at 1593 and 1525 cm^{-1} are indicative of the stretching vibrations of C=C bonds in the benzenoid and quinoid rings, respectively. A notable alteration is evident at 1482 cm^{-1} band, which is attributed to the C=N stretching of the quinoid units and exhibits a significant shift for samples S2 and S3. Furthermore, there is a band located at ~1403 cm^{-1}, which corresponds to the stretching of quinoid C-C bonds in PANI. The band at 1333 cm^{-1} is attributed to the radical cation (C-$N^{+\bullet}$ stretching) [23,24] and likewise demonstrates a shift at higher fluences. Additionally, the band at 1245 cm^{-1} corresponds to the stretching of benzenoid C-N bonds in PANI. Furthermore, a blue shift at 1171 cm^{-1} band for the PANI in the S2 thin film. This particular band is attributed to the C-H in-plane deformation mode of the quinoid units within PANI [25]. Additionally, there are other bands in the spectrum, notably around 813 cm^{-1}, which likely correspond to amine deformations [26]. Therefore, Raman spectra serve as confirmation of the successful creation of composite thin films and the more pronounced shifting observed in films irradiated at fluences higher than 1×10^{10} ions/cm^2 signifies structural alterations in the PANI/ZnO nanocomposite thin films at these elevated fluences.

SEM-EDS studies: The morphologies of the PANI/ZnO nanocomposite thin films were scrutinized through scanning electron microscopy (SEM) and elemental analysis was conducted using energy-dispersive spectroscopy (EDS). From the SEM images (Fig. 3a-e), it is observed that the synthesized films are in the form of interconnected nanofibers along with the pseudo-spherical shape indicating the presence of ZnO [27]. As the fluence ions concentration increased, no alterations in morphology were observed; nevertheless, it was observed that the nanostructures began to coalesce. The diameters of

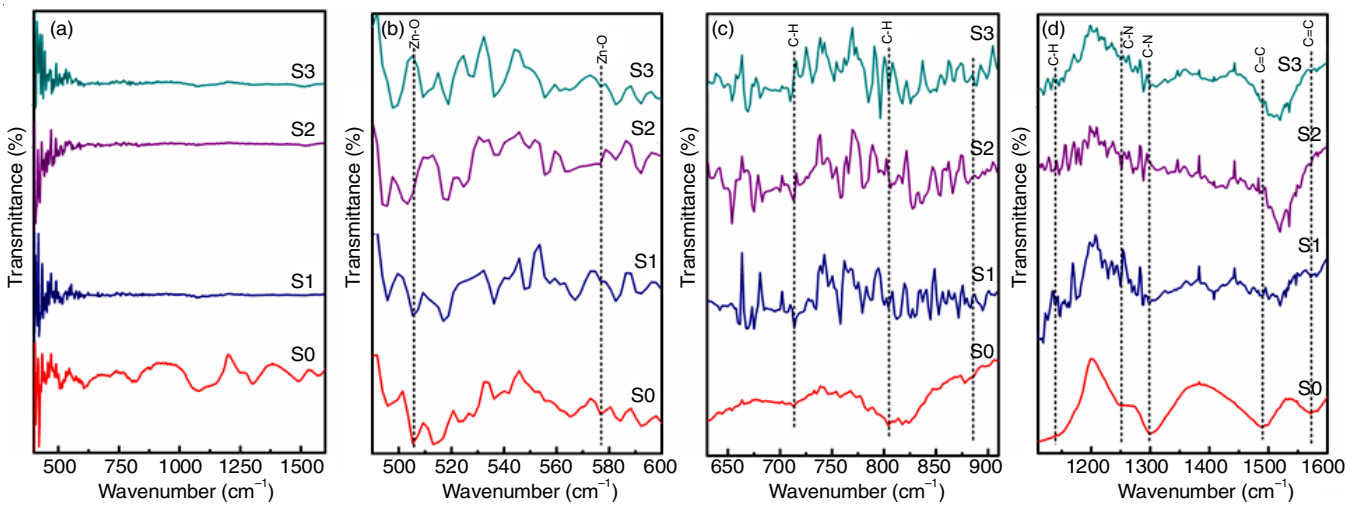

Fig. 1. FT-IR patterns at range (a) 400-1600 cm^{-1}, (b) 490-600 cm^{-1}, (c) 690-910 cm^{-1}, (d) 1100-1600 cm^{-1} of pure and irradiated PANI/ZnO nanocomposite thin films

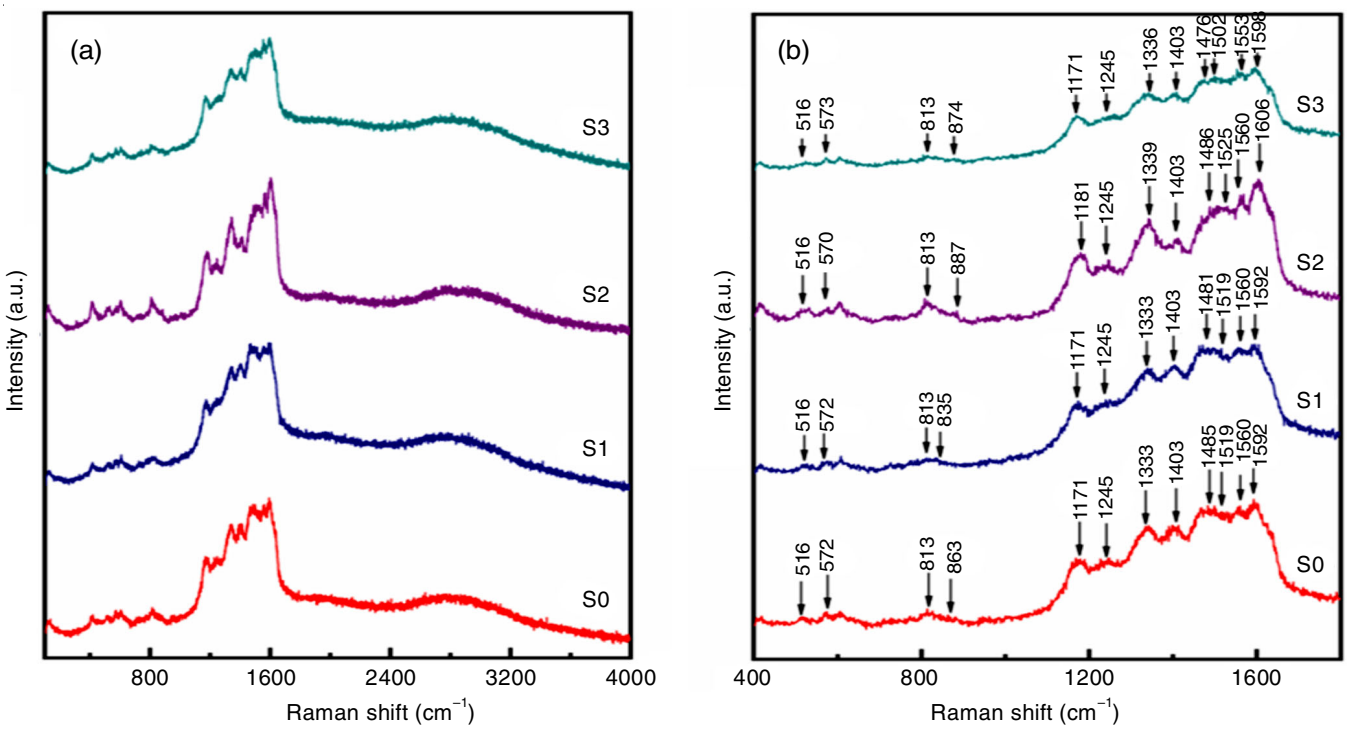

Fig. 2. Raman spectra within range (a) 400-4000 cm^{-1} and (b) 400-1800 cm^{-1} of pure and irradiated PANI/ZnO nanocomposite thin films

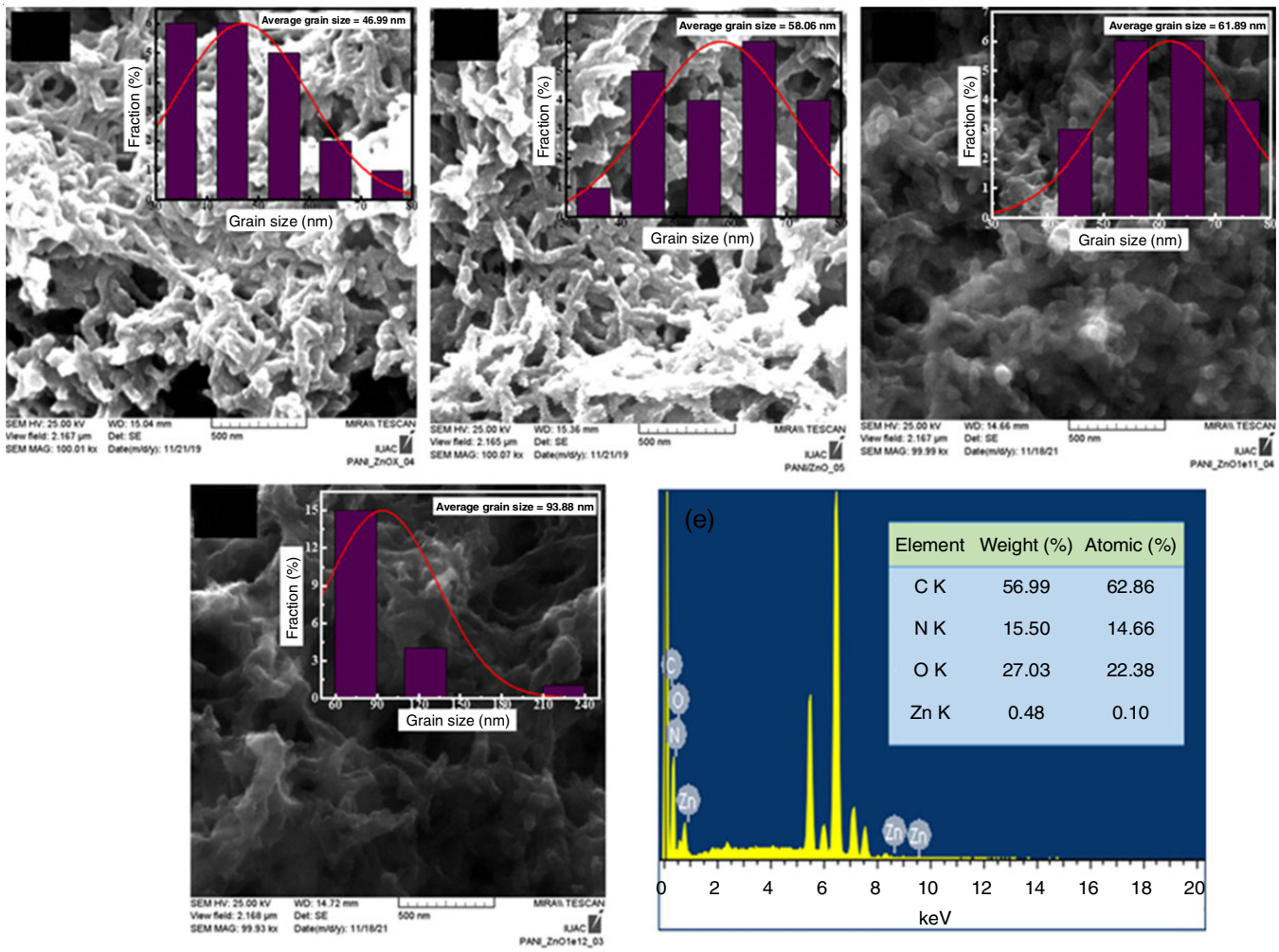

Fig. 3. (a-d) represents the SEM micrographs of S0, S1, S2 and S3 samples whereas (e) shows EDS spectra of Pristine PANI/ZnO nanocomposite

the nanofibers exhibited an increase with the rising ion fluence concentrations. This augmentation in diameter, progressing from 47 nm in the pristine film to 98 nm in the film subjected to the highest fluence irradiation, can be attributed to agglomeration. The increase in diameter, leading to agglomeration of the nanofibers, is induced by the occurrence of hydrogen bonds.

These bonds arise due to interactions between ZnO and N-H groups or coordination bonds [28,29]. The effects of fluence ions concentrations on the morphology of thin films are investi-gated. The EDS spectra affirm the existence of C, O, N and Zn elements, each accompanied by their anticipated atomic and weight percentages. These findings are presented in the table featured within the EDS spectra, as seen in Fig. 3e. The SEM images have played a pivotal role in affirming both the success-ful synthesis of PANI/ZnO nanocomposite thin films and the discernible alterations in morphology linked to varying ion fluence concentrations.

Dark I-V study using space charge limited current (SCLC) method: The SCLC method is a technique that widely used to probe transport properties of semiconductor materials by injecting unipolar charge carrier (electron or hole) in the material. Dark I-V measurements were performed on single carrier devices for pristine and irradiated samples of PANI-ZnO nanocomposite of thickness ~6 μm at different fluence of 100 MeV Ag^{10+} ions. The transport parameters of hole type single carrier device (Ag/PANI-ZnO/Ag) were extracted using SCLC method.

In SCLC method, dark I-V characteristics divided into three regions as (i) Ohmic region, (ii) trap filled region and (iii) child's region. The Ohmic response observed at low bias and shows the linear ($I = V^n$, $n = 1$) behaviour. This conductive behaviour is attributes to present background charge carriers in the materials [30]. When the injected charge carrier density overcomes the present charge carrier in the material, then the trap states start filling. The I-V characteristics shows the sharp rise in dark current in intermediate region. This intermediate I-V response corresponds to the trap filled region ($I = V^n$, $n > 2$). After filling all the trap states, the injected charge carrier starts building up that leads to current saturation and exhibits quadratic behaviour ($I = V^n$, $n = 2$). This region is called childs region [31].

Fig. 4 shows the dark I-V curves for pristine and irradiated samples of Ag/PANI-ZnO/Ag hole type device in forward and revers bias scan. The sample were irradiated by Ag^{10+} of 100 MeV energy with different fluence (S0 = 0, S1 = 10^{10} ions/cm^2, S2 = 10^{11} ions/cm^2, S3 = 10^{12} ions/cm^2). The I-V characteristics exhibit well correlation with the energy level alignment as shown in schematic diagram (Fig. 5) for single carrier device. The exhibited dark current curves are nearly symmetric. However, a slight variation in current saturation is observed that can be attributes to present of trap states. For S1 and S2 samples, the dark current saturation (~5 × 10^{-4} A) was observed slightly at higher values compare to the S0 (~5 × 10^{-5} A). However, S3 sample shows drop in saturation current (~5 × 10^{-5} A to ~5 × 10^{-6} A) that can be attributes with the sample degradation upon ion irradiation of high fluence rate.

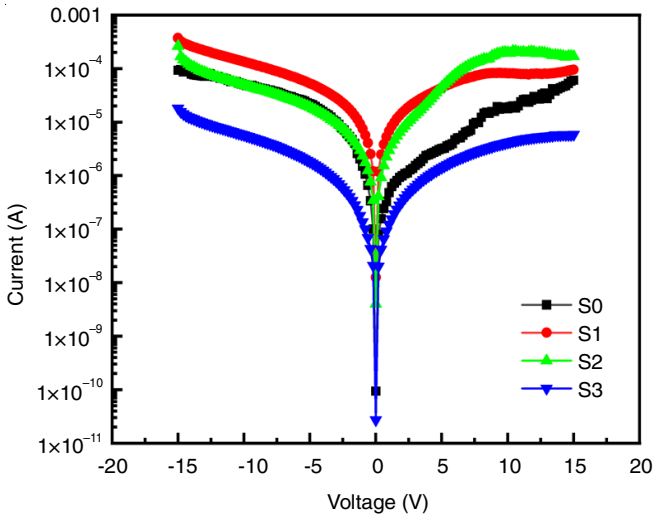

Fig. 4. Dark I-V characteristics for hole type device (Ag/PANI-ZnO/Ag)

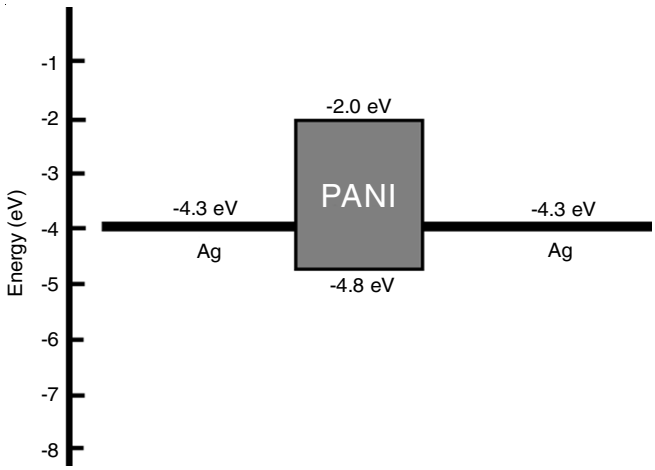

Fig. 5. Band-bending diagram of the materials utilized in the device

Fig. 6 shows the hysteresis I-V scans for hole type device of pristine and irradiated samples. The forward and reverse I-V scan of pristine sample S0, shows a significant hysteresis. However, for irradiated samples S1 and S3, the curves show reduction or very minimal signature of hysteresis. The irradiation of Ag^{10+} ions have shown a suppression of hysteresis curve that can be associated with reduction in influence of trap states on carrier transport.

From Fig. 7, the dark I-V curves the conductivity (σ), trap states density (N_{trap}), hole mobility (μ) and carrier concentration (N_c) of the material were calculated using SCLC method.

From Ohmic region the conductivity was calculated using eqn. 1:

$$\sigma = \frac{\Delta I}{L \Delta V} \quad (1)$$

where I is the current and V is the applied voltage, L is the thickness of the device. The conductivity values were in the range of 5.97 × 10^{-4} S/cm to 1.13 × 10^{-2} S/cm. For S1 sample the conductivity was enhanced at low fluence (~10^{10} ions/cm^2). However, for S3 sample the reduction in conductivity up to ~1.76 × 10^{-4} S/cm compared to the S0 sample was observed. The ion irradiation has shown the significant effect as it leads

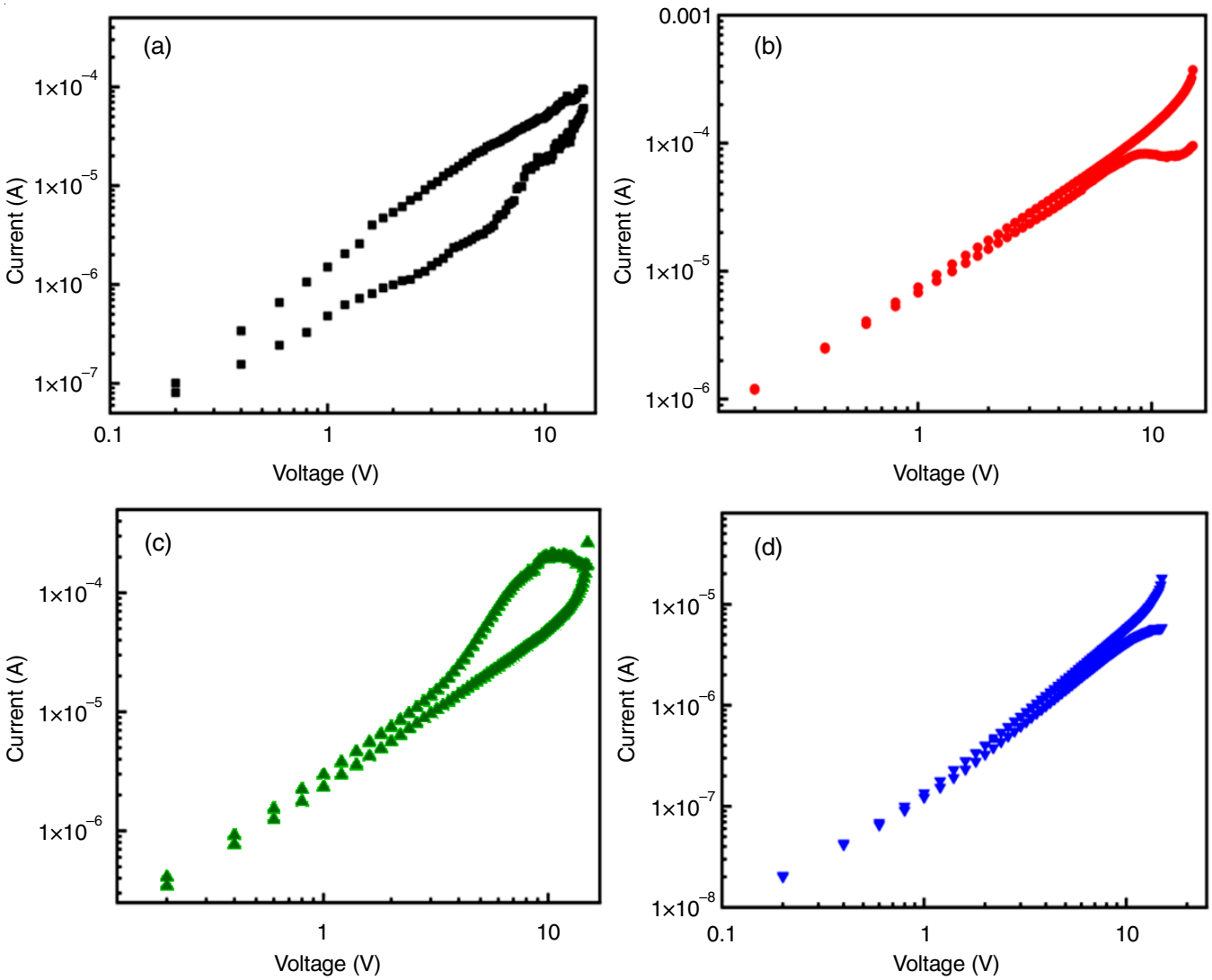

Fig. 6. I-V hysteresis curves for hole type devices in forward and reverse bias of (a) S0, (b) S1, (c) S2 and (d) S3 samples

to rise in conductivity of the order of 10^2 in sample S1. Trap states density N_{trap} was calculated using eqn. 2, from the intermediate bias trap filled region:

$$N_{trap} = \frac{2\varepsilon_o \varepsilon V_{TFL}}{qL^2} \quad (2)$$

where ε_o is the free space permittivity, ε (= 674) [32] is the relative permittivity or dielectric constant, L is the device thickness, V_{TFL} is the trap filled voltage and q charge (hole). For pristine sample S0, the calculated trap states were 1.58×10^{16} cm^{-3}. However for samples S1 and S3, no trap states were observed that can be associated with reduction in trap states on ion irradiation. The hole mobility was calculated from the dark saturation current and corresponding applied voltage in the child's region ($I\text{-}V^n$, n = 2). The recorded quadratic I-V response was studied using the Mott-Gurney (M-G) relation (eqn. 3) [31].

$$\mu = \frac{8}{9}\frac{J_D L^3}{V^2 \varepsilon \varepsilon_o} \quad (3)$$

where V is the voltage applied corresponds to child's region, J_D is dark current density, L is the device thickness, ε is the relative dielectric constant, ε_o is free space permittivity. The fabricated hole type device was in well correlation with the Mott-Gurney's limitations: (i) there should be Ohmic contact between metal and semiconductor junction and the potential barrier should be as low as possible; (ii) there should be no trap states in the materials and (iii) to probe the transport properties of the material, there should be unipolar carrier injection either electron or hole. For the fabricated device, the Fermi level of used Ag metal as electrode was nearly aligned with the valence band minima of the used active PANI-ZnO nanocomposite semiconductor material (Fig. 4). There was no significant change in mobility values were observed on irradiation, except S2 sample that shows rise in mobility as compared to the S0, S1 and S3 samples (Table-1). The hole mobility values were well correlated with previous published reports. However, the mobility shows higher values by one order of magnitude (~10^{-6} cm^2/V-s) in compared to the reported mobility values (~10^{-7} cm^2/V-s) for PANI/Si heterostructure, measured by using space charge limited current method [4].

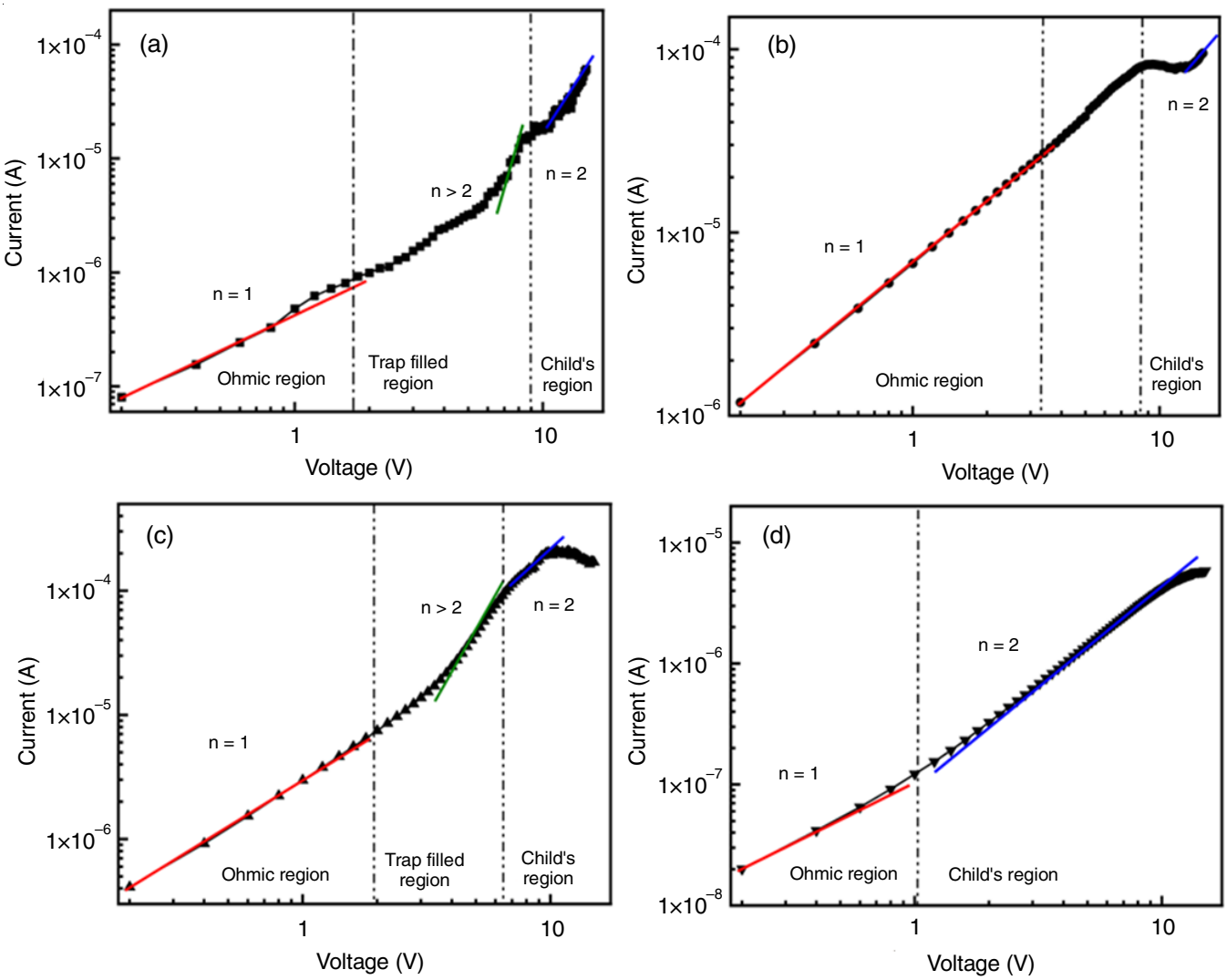

Fig. 7. Dark I-V curves for hole type device of (a) S0, (b) S1, (c) S2 and (d) S3 samples

TABLE-1
TRANSPORT PARAMETERS EXTRACTED FROM THE DARK I-V USING SCLC METHOD

Sample	Fluence of Ag^{10+} of 100 MeV (ions/cm^2)	Conductivity σ (S/cm)	Trap states N_{trap} (cm^{-3})	Mobility μ (cm^2/V-s)	Carrier concentration N_c (cm^{-3})
S0	0	5.97×10^{-4}	1.58×10^{16}	3.21×10^{-6}	1.16×10^{21}
S1	10^{10}	1.14×10^{-2}	NA	7.09×10^{-6}	1.04×10^{22}
S2	10^{11}	4.68×10^{-3}	1.14×10^{16}	3.56×10^{-5}	8.02×10^{20}
S3	10^{12}	1.76×10^{-4}	NA	7.54×10^{-7}	1.45×10^{21}

The carrier concentration was calculated using eqn. 4:

$$N_c = \frac{\sigma}{\mu . q} \quad (4)$$

where σ is the conductivity, μ is the mobility and q is the elementary charge. The materials exhibited higher carrier concentration ranging from ~8×10^{20} cm^{-3} to 1×10^{23} cm^{-3}. The calculated carrier concentration was comparably higher than the reported reports [4].

From the dark I-V measurements using SCLC method, the calculated transport parameters have showed the enhancement in their transport properties for irradiated samples at low fluence. However, at high fluence for sample S3 the significant reduction in transport properties were observed compared to the pristine and irradiated sample at low fluence. In this study, the ion irradiation showed the change in transport properties in composite samples of organic semiconductor PANI and ZnO nanoparticle. This finding suggests that further studies and better understanding of ion irradiation and its effect on organic semiconductors can be of great interest. As in recent times, in the field of polymer based optoelectronic device a significant growth has been observed due to their flexibility, low cost and easy processing [33-37]. The organic based solar cells are being widely used as transparent and opaque solar cell on widows and sheets. This study can help in further optimization of organic solar cell device and other optoelectronic devices [1,38-41].

Conclusion

The PANI/ZnO nanocomposite films were successfully fabricated by electrochemical method. The samples were irradiated by 100 MeV Ag^{10+} ions at different fluences in the range of 10^{10} to 10^{12} ions/cm^2. The structural properties and associated vibrational modes were analyzed by using FTIR and Raman spectroscopic techniques. The morphological features were also observed using SEM-EDS. The combined results of FTIR and Raman analyses offer confirmation of the successful synthesis of PANI/ZnO nanocomposite thin films. The shifts in vibrational modes (Zn-O, C-H bond) towards lower wavenumbers were observed. The vibrational shifts were particularly prominent in the films irradiated with doses exceeding 1×10^{10} ions/cm^2. The SEM analysis provides valuable insights into the morphology and grain size effects, thereby corroborating the findings mentioned above, moreover, also exhibited the uniform coating of ZnO on PANI matrix. The dark I-V study using SCLC method has exhibited the enhancement in transport properties in samples S1 and S2 irradiated at low fluence. The conductivity (S1 ~ 1.14×10^{-2} S/cm) and mobility (S2 ~ 3.56×10^{-5} cm^2/V-s) values were enhanced as compared to pristine sample (S0). This study suggests that the reported nanocomposite of PANI/ZnO can be used a potential candidate in optoelectronic devices.

ACKNOWLEDGEMENTS

The authors are thankful to the Inter University Accelerator Centre, New Delhi, India for providing the electrodeposition and characterization facilities. The authors also thank Indira Gandhi Delhi Technical University for Women, Delhi, India for providing the FTIR characterization facility.

CONFLICT OF INTEREST

The authors declare that there is no conflict of interests regarding the publication of this article.

REFERENCES

1. M. Beygisangchin, S.A. Rashid, S. Shafie, A.R. Sadrolhosseini and H.N. Lim, *Polymers*, **13**, 2003 (2021); https://doi.org/10.3390/polym13122003
2. J. Heck, J. Goding, R. Portillo Lara and R. Green, *Acta Biomater.*, **139**, 259 (2022); https://doi.org/10.1016/j.actbio.2021.05.052
3. M.R. Waikar, A.A. Shaikh and R.G. Sonkawade, *Polym. Bull.*, **76**, 4703 (2019); https://doi.org/10.1007/s00289-018-2634-1
4. J. Toušek, J. Toušková, R. Chomutová, I. Køivka, M. Hajná and J. Stejskal, *Synth. Met.*, **234**, 161 (2017); https://doi.org/10.1016/j.synthmet.2017.10.015
5. A. Kolodziejczak-Radzimska and T. Jesionowski, *Materials*, **7**, 2833 (2014); https://doi.org/10.3390/ma7042833
6. Y. Zhang, M.K. Ram, E.K. Stefanakos and D.Y. Goswami, *J. Nanomater.*, **2012**, 624520 (2012); https://doi.org/10.1155/2012/624520
7. T. Alamgeer, M. Tahir, M.R. Sarker, S. Ali, Ibraheem, S. Hussian, S. Ali, M. Imran Khan, D.N. Khan, R. Ali and S. Mohd Said, *Polymers*, **15**, 363 (2023); https://doi.org/10.3390/polym15020363
8. A.M. Mohammed, S.S. Mohtar, F. Aziz, M. Aziz and A. Ul-Hamid, *J. Environ. Chem. Eng.*, **9**, 105065 (2021); https://doi.org/10.1016/j.jece.2021.105065
9. K. Daideche, L. Hasniou and D. Lerari, *Chem. Proc.*, **3**, 110 (2021); https://doi.org/10.3390/ecsoc-24-08328
10. S. Sivakumar, Y. Robinson and N.A. Mala, *Appl. Surf. Sci. Adv.*, **12**, 100344 (2022); https://doi.org/10.1016/j.apsadv.2022.100344
11. A. Kumar and S. Banerjee, *Int. J. Nanosci.*, **10**, 161 (2011); https://doi.org/10.1142/S0219581X11007442
12. A. Ibrayeva, A. Mutali, J. O'Connell, A.J. van Vuuren, E. Korneeva, A. Sohatsky, R. Rymzhanov, V. Skuratov, L. Alekseeva and I. Ivanov, *Nuclear Materials and Energy*, **30**, 101106 (2022); https://doi.org/10.1016/j.nme.2021.101106
13. M. Pandian, A. Krishnaprasanth, M. Palanisamy, G. Bangaru, R. Meena, C.L. Dong and A. Kandasami, *Nanomaterials*, **12**, 3782 (2022); https://doi.org/10.3390/nano12213782
14. K. Kaur, *J. Phys.: Conf. Series*, **2267**, 012111 (2022); https://doi.org/10.1088/1742-6596/2267/1/012111
15. G.B. Patel, N.L. Singh, F. Singh and P.K. Kulriya, *Radiat. Phys. Chem.*, **181**, 109288 (2021); https://doi.org/10.1016/j.radphyschem.2020.109288
16. Z. Aftab, I. Sulania, A. Kandasami and L. Nair, *ACS Omega*, **7**, 31869 (2022); https://doi.org/10.1021/acsomega.2c02653
17. A. Hussain, Shumaila, A. Dhillon, I. Sulania and A.M. Siddiqui, Eds.: V. Singh, R. Sharma, M. Mohan, M.S. Mehata and A.K. Razdan, Comparative Study of Polypyrrole/Zinc Oxide Nanocomposites Synthesized by Different Methods, In: Proceedings of the International Conference on Atomic, Molecular, Optical & Nano Physics with Applications: CAMNP 2019, Singapore: Springer Singapore, pp. 601-607 (2022).
18. M.L. da Silva-Neto, M.C. de Oliveira, C.T. Dominguez, R.E. Lins, N. Rakov, C.B. de Araújo, L.D.S. Menezes, H.P. de Oliveira and A.S. Gomes, *Sci. Rep.*, **9**, 11765 (2019); https://doi.org/10.1038/s41598-019-48056-w
19. A. Batool, F. Kanwal, M. Imran, T. Jamil and S.A. Siddiqi, *Synth. Met.*, **161**, 2753 (2012); https://doi.org/10.1016/j.synthmet.2011.10.016
20. L. Jiang and Z. Cui, *Polym. Bull.*, **56**, 529 (2006); https://doi.org/10.1007/s00289-005-0494-y
21. S.S. Liu, L.J. Bian, F. Luan, M.T. Sun and X.X. Liu, *Synth. Met.*, **162**, 862 (2012); https://doi.org/10.1016/j.synthmet.2012.03.015
22. D. Wang and F. Caruso, *Adv. Mater.*, **13**, 350 (2001); https://doi.org/10.1002/1521-4095(200103)13:5<350::AID-ADMA350>3.0.CO;2-X
23. T. Fukuda, H. Takezoe, K. Ishikawa, A. Fukuda, H.S. Woo, S.K. Jeong, E.J. Oh and J.S. Suh, *Synth. Met.*, **69**, 175 (1995); https://doi.org/10.1016/0379-6779(94)02409-R
24. J.P. Da Silva, S.C. De Torresi, D.L.A. De Faria and M.L.A. Temperini, *Synth. Met.*, **101**, 834 (1999); https://doi.org/10.1016/S0379-6779(98)01300-9
25. G. Louarn, M. Lapkowski, S. Quillard, A. Pron, J.P. Buisson and S. Lefrant, *J. Phys. Chem.*, **100**, 6998 (1996); https://doi.org/10.1021/jp953387e
26. Q. Hao, W. Lei, X. Xia, Z. Yan, X. Yang, L. Lu and X. Wang, *Electrochim. Acta*, **55**, 632 (2010); https://doi.org/10.1016/j.electacta.2009.09.018
27. J. Shen, M. Shi, B. Yan, H. Ma, N. Li and M. Ye, *J. Mater. Chem.*, **21**, 7795 (2011); https://doi.org/10.1039/c1jm10671f
28. N.S. Singh, L. Kumar, A. Kumar, S. Vaisakh, S.D. Singh, K. Sisodiya, S. Srivastava, M. Kansal, S. Rawat, T.A. Singh, Tanya and Anita, *Mater. Sci. Semicond. Process.*, **60**, 29 (2017); https://doi.org/10.1016/j.mssp.2016.12.021
29. J. Stejskal, I. Sapurina and M. Trchová, *Prog. Polym. Sci.*, **35**, 1420 (2010); https://doi.org/10.1016/j.progpolymsci.2010.07.006
30. E.A. Duijnstee, V.M. Le Corre, M.B. Johnston, L.J.A. Koster, J. Lim and H.J. Snaith, *Phys. Rev. Appl.*, **15**, 014006 (2021); https://doi.org/10.1103/PhysRevApplied.15.014006

31. M. Warish, G. Jamwal, Z. Aftab, N. Bhatt and A. Niazi, Preprint (2023); https://doi.org/10.48550/arXiv.2304.12701
32. K. Daideche, L. Hasniou and D. Lerari, *Chem. Proc.*, **3**, 110 (2020); https://doi.org/10.3390/ecsoc-24-08328
33. S. Li, D. Huang, B. Zhang, X. Xu, M. Wang, G. Yang and Y. Shen, *Adv. Energy Mater.*, **4**, 1301655 (2014); https://doi.org/10.1002/aenm.201301655
34. P. Wan, X. Wen, C. Sun, B.K. Chandran, H. Zhang, X. Sun and X. Chen, *Small*, **11**, 5409 (2015); https://doi.org/10.1002/smll.201501772
35. L. Zhang, P. Wan, T. Xu, C. Kan and M. Jiang, *Opt. Express*, **29**, 19202 (2021); https://doi.org/10.1364/OE.430132
36. T. Yin, Y. Cheng, Y. Hou, L. Sun, Y. Ma, J. Su, Z. Zhang, N. Liu, L. Li and Y. Gao, *Small*, **18**, 2204806 (2022); https://doi.org/10.1002/smll.202204806
37. B. Yao, L. Yuan, X. Xiao, J. Zhang, Y. Qi, J. Zhou, J. Zhou, B. Hu and W. Chen, *Nano Energy*, **2**, 1071 (2013); https://doi.org/10.1016/j.nanoen.2013.09.002
38. Z. Liu, J. Zhou, H. Xue, L. Shen, H. Zang and W. Chen, *Synth. Met.*, **156**, 721 (2006); https://doi.org/10.1016/j.synthmet.2006.04.001
39. E. Shanmugasundaram, C. Govindasamy, M.I. Khan, V. Ganesan, V. Narayanan, K. Vellaisamy, R. Rajamohan and S. Thambusamy, *Carbon Letters*, (2023); https://doi.org/10.1007/s42823-023-00578-0
40. A.K. Sharma, A.K. Sharma and R. Sharma, *Bull. Mater. Sci.*, **44**, 121 (2021); https://doi.org/10.1007/s12034-021-02388-4
41. P. Liu and L. Zhang, *Crit. Rev. Solid State Mater. Sci.*, **34**, 75 (2009); https://doi.org/10.1080/10408430902875968